27

Semiconductor Bloch Equations

By R. v. Baltz

The electrodynamic description of matter requires constitutive equations that relate the induced charge ρ and current density $\boldsymbol{j}$ of the semiconductor (or, equivalently, the polarization $\boldsymbol{P}$, with $\boldsymbol{j} = \dot{\boldsymbol{P}}$ and $\rho = -\mathrm{div}\boldsymbol{P}$) to the electromagnetic fields $\boldsymbol{E}, \boldsymbol{B}$. Generic models in this respect are the Lorentz-oscillator and the Drude free-carrier model of linear optics that have already been extensively used in Chaps. 4, 5, and 11–13. The description of nonlinear properties of matter, on the other hand, mostly uses a power series expansion of the polarization in terms of the electrical field (see Chap. 19). Such an expansion, however, is inappropriate under resonant or near-resonant conditions. In some cases new solutions may even arise "spontaneously" above a critical light field and can lead to second harmonic generation although a power expansion (including even-order terms with respect to the light field) does not exist. Therefore, a realistic description of semiconductor optics requires the proper dependence on the light field, the inclusion of the valence conduction band continuum states, exciton effects, as well as band-filling dynamics. These phenomena are consistently described by the *Semiconductor Bloch-Equations* (SBEs), which have become the standard model for semiconductor optics. [1] In this approach the semiconductor is treated quantum mechanically leads to a set of coupled nonlinear differential equations for the polarization and the electron/hole distribution functions (supplemented by higher order correlation functions, which will be omitted here). The polarization acts as a source term in the (classical) Maxwell equations as discussed in Chap. 2. In this sense, the SBEs are a semiclassical theory. It successfully covers linear as well as nonlinear phenomena such as pump-probe, four-wave-mixing, or photon echo experiments (see Chaps. 20– 25).

[1] The main idea of the SBEs originates from Bloch's seminal work on the theory of (nuclear) spin resonance [46B1] and Haken's theory of the laser [70H1]. For semiconductors, the band-edge equations were first studied by Stahl [84S1] and subsequently developed, by Haug and his coworker and colleagues [94H1] and others, into a powerful tool for semiconductor theory.

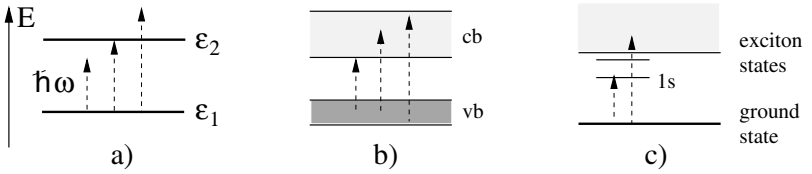

Fig. 27.1. Route for a qualitative derivation of the the semiconductor Bloch equations. (**a**) Two-level system (resonant and nonresonant excitation) (**b**) Noninteracting valence and conduction bands viewed as a collection of TLSs with different transition energies (**c**) Two interacting bands including some bound exciton states

The SBEs are of considerable complexity in derivation and application, therefore, we shall give only a "pedestrian version" of their derivation and some selected applications. Details can be found in Haug and Koch's textbook [94H1]. For a recent comprehensive presentation of the SBEs see, e.g., Schäfer and Wegener's book [02S1]. We approach the problem in three steps as sketched in Fig. 27.1

1. First we study the dynamics of atoms near resonance in the two-level approximation and derive the optical Bloch equations. In this formulation, damping processes can also be included on a phenomenological level.
2. Second, we generalize this result for a two-band model of a direct semiconductor omitting the Coulomb interaction between electrons and holes. In this description the semiconductor is sketched as a collection of noninteracting two-level systems (TLSs).
3. Finally, we add the Coulomb interaction between the electrons and holes, which includes exciton and screening effects. This will lead us to the SBEs in their simplest form, including excitons or the transition to an electron hole plasma.

27.1 Dynamics of a Two-Level System[2]

Near the resonance of an atomic transition, $\omega \approx \omega_0 = (\epsilon_2 - \epsilon_1)/\hbar$, we may only retain the pair of nearly resonant stationary states $|1\rangle$ and $|2\rangle$ with energies ϵ_1 and ϵ_2, $(\epsilon_2 > \epsilon_1)$, between which the transition occurs (see Fig. 27.1a). In this two-level approximation, the wave function

$$|\,\psi(t)\rangle = c_1(t)|1\rangle + c_2(t)|2\rangle \tag{27.1}$$

[2] The dynamics of a TLS is very well presented in many texts, in particular Allen and Eberly's classic book on optical resonance and two-level atoms [87A1] or the textbooks *The Feynman Lectures*, Vol. III, in connection with the Ammonia maser [64F1] and *Licht und Materie* by Haken [70H1]. Note the different enumeration of states.

is described by coefficients c_1, c_2, which may be arranged as a column vector $\boldsymbol{c}$, the time-dependence of which is governed by the Schrödinger equation

$$i\hbar\frac{\partial}{\partial t}\begin{pmatrix} c_1 \\ c_2 \end{pmatrix} = \widehat{H}\begin{pmatrix} c_1 \\ c_2 \end{pmatrix}. \tag{27.2}$$

In addition, we assume that the optical transition between $|1\rangle$ and $|2\rangle$ is dipole-allowed and the light is polarized parallel to the z-axis. As a result, the Hamiltonian reads

$$\widehat{H} = \widehat{H}_0 - \widehat{d}E_z(t), \qquad \widehat{H}_0 = \begin{pmatrix} \epsilon_1 & 0 \\ 0 & \epsilon_2 \end{pmatrix}, \qquad \widehat{d} = \begin{pmatrix} 0 & d^* \\ d & 0 \end{pmatrix}. \tag{27.3}$$

$\widehat{H}_0$ and $\widehat{d}$ denote the Hamiltonian of the isolated atom and the electric dipole operator with $d = \langle 2| - ez|1\rangle$, respectively (see also Sect. 3.2.2).

From $c_1(t), c_2(t)$ the induced dipole moment $d(t)$ and the population inversion $I(t)$ of the TLS are determined by

$$d(t) = \mathbf{c}^\dagger \widehat{d}^* \mathbf{c} = 2\,\mathrm{Re}\left[d^*\,\mathcal{P}(t)\right], \tag{27.4}$$

$$I(t) = |c_2(t)|^2 - |c_1(t)|^2, \quad \text{and} \tag{27.5}$$

$$\mathcal{P}(t) = c_1^*(t)c_2(t), \tag{27.6}$$

where $\mathcal{P}(t)$ is the (dimensionless) complex dipole moment.[3] ϵ_1, ϵ_2 and d are considered as parameters of this model. There are at least three ways to tackle the problem. These will be discussed in the next sections.

27.1.1 Wave-Function Description

We start with a pure state described by (27.1) and factor off the time dependence of the state vector without an external field (interaction picture),

$$c_j(t) = a_j(t)e^{-\imath\epsilon_j t/\hbar}, \quad j = 1, 2, \tag{27.7}$$

where $a_j(t)$ obey the differential equations

$$\dot{a}_1(t) = i\frac{d^*}{\hbar}\,E_z(t)\,e^{-i\omega_0 t}a_2(t), \tag{27.8}$$

$$\dot{a}_2(t) = i\frac{d}{\hbar}\,E_z(t)\,e^{+i\omega_0 t}a_1(t). \tag{27.9}$$

Equations (27.8,27.9) are linear and first order. Nevertheless, no analytical solution is achievable. However, for a monochromatic field with frequency ω near resonance, $\omega \approx \omega_0$, the product of $E_z(t) = E_0\cos(\omega t)$ and $e^{\pm i\omega_0 t}$, respectively, contain a term that is almost constant and another that oscillates

[3] Haug and Koch [94H1] use a reverse notation concerning $\boldsymbol{P}$ and $\mathcal{P}$.

rapidly. The first term drives the system coherently whereas the fast oscillating term almost averages to zero, which will be neglected in the following. For reasons that will become obvious later, this approximation is called the rotating wave approximation (RWA). Within the RWA, (27.8,27.9) become

$$\dot{a}_1(t) = i\frac{\omega_R^*}{2}\, e^{+i\delta t} a_2(t), \tag{27.10}$$

$$\dot{a}_2(t) = i\frac{\omega_R}{2}\, e^{-i\delta t} a_1(t), \tag{27.11}$$

which (besides ω and ω_0) contain two characteristic frequencies

- $\omega_R = d\,E_0/\hbar$, the *Rabi frequency* (real, for simplicity) and
- $\delta = \omega - \omega_0$, which is called the "detuning" frequency.

By insertion, (27.10,27.11) lead to an equation of motion for a harmonic oscillator with "imaginary damping"

$$\ddot{a}_1(t) - i\delta\dot{a}_1(t) + (\frac{\omega_R}{2})^2 a_1(t) = 0\,, \tag{27.12}$$

which can be solved by the standard exponential ansatz. For example, at resonance, $\delta = 0$, and initial conditions $a_1(0) = 1$, $a_2(0) = 0$, we have

$$a_1(t) = \cos(\frac{\omega_R}{2}t), \quad a_2(t) = i\sin(\frac{\omega_R}{2}t). \tag{27.13}$$

Hence, the probability of finding the TLS in the excited state, $|c_2(t)|^2 = |a_2(t)|^2$, oscillates with the Rabi frequency ω_R. The same holds true for the population inversion, (see Fig. 27.2). At time $t_1 = \pi/\omega_R$ the atom is in the excited state and at $2\pi/\omega_R$ it is back in the ground state. This is called *Rabi flopping*. For detuned fields, the solution of (27.12) displays incomplete Rabi flopping where the period becomes shorter and the amplitude is smaller than when on resonance. See also Sect. 23.2.2.3.

A numerical example may be found, e.g., in Boyd [92B1]. For atomic sodium the parameters for the $3s-3p$ transition are: $d = 2.5a_Be$, $\lambda_0 = 589\,\mathrm{nm}$

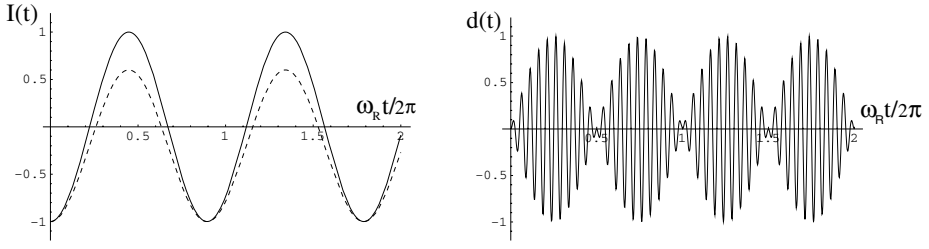

Fig. 27.2. Rabi oscillations of the inversion (*left*) and induced dipole moment (*right*). Resonant excitation (*solid line*), detuned excitation at $\omega = 0.5\omega_0$ (*dashed line*), $\omega_R = 0.05\omega_0$

(a_B is the Bohr radius). For an intensity of $127\,\mathrm{W\,cm^{-2}}$ (which can be easily realized by focusing a low power laser beam) the Rabi frequency $\omega_R/2\pi \approx 1\,\mathrm{GHz}$ becomes larger than the natural line width and oscillations will appear. For further examples see, e.g., Di Bartolo's article [05B1].

27.1.2 Polarization and Inversion as State Variables

Instead of c_1, c_2 one can likewise use the inversion $I(t)$ and the complex polarization $\mathcal{P}(t)$ themselves as state variables which – remarkably – obey a closed set of first order differential equations. Using (27.5,27.6) together with (27.8,27.9) we obtain (even without RWA)

$$\left[\frac{\mathrm{d}}{\mathrm{d}t} + i\omega_0\right] \mathcal{P}(t) = -i\omega_R(t)\, I(t) + \dot{\mathcal{P}}_{\mathrm{rel}}, \tag{27.14}$$

$$\frac{dI(t)}{dt} = -4\,\mathrm{Im}\,\left[\omega_R(t)\mathcal{P}^*(t)\right] + \dot{I}_{rel}, \tag{27.15}$$

$$\omega_R(t) = \frac{d}{\hbar} E_z(t). \tag{27.16}$$

$\omega_R(t)$ is the instantaneous Rabi frequency. (In the following, d as well as $\omega_R(t)$, can be assumed to be real).

The advantage of this description with respect to (27.8,27.9) is the possibility to include damping (i.e., incoherent interactions with a "bath") in a phenomenological way just by adding relaxation terms, which is not possible to do for (27.8,27.9)[4]:

$$\dot{\mathcal{P}}_{rel} = -\frac{\mathcal{P}}{T_2}, \quad \dot{I}_{rel} = -\frac{I(t) - I_{\mathrm{eq}}}{T_1}. \tag{27.17}$$

T_1 and T_2 determine the population (or energy) and phase relaxation of the TLS and they are also called longitudinal and transverse relaxation times. (The notation will become clear at the end of the next section). As I is the square of an amplitude, we may expect $T_2 = 2T_1$. However, there are always phase disturbing processes that do not contribute to energy relaxation so that in general $T_2 \leq 2T_1$. In semiconductors, one finds frequently that $T_2 \ll 2T_1$. I_{eq} is the equilibrium value of the inversion in the absence of the driving field, e.g., at zero temperature $I_{\mathrm{eq}} = -1$. See also Sect. 23.1.

Without damping, there is a conserved quantity,

$$4\,|\mathcal{P}(t)|^2 + I^2(t) = \mathrm{const}\,, \tag{27.18}$$

which may be used to eliminate the inversion from (27.14). Its origin becomes obvious from a remarkable analogy between any TLS and a spin-1/2 system in a magnetic field as discussed in the following subsection.

[4] A microscopic treatment of relaxation processes requires a density matrix approach or equivalent formulations. $I(t)$ contains the diagonal elements of the density operator, $\rho_{jj} (= |c_j|^2)$, whereas $\mathcal{P}(t)$ probes the off-diagonal element $\rho_{12} (= c_1^* c_2)$.

27.1.3 Pseudo-Spin Formulation

The Hamiltonian of a single spin-1/2 in a magnetic field $\boldsymbol{B}$ reads

$$\widehat{H} = -g\frac{\mu_B}{\hbar}\,\widehat{S}\boldsymbol{B} = -\mu_B \boldsymbol{B}\widehat{\sigma}, \tag{27.19}$$

where $\widehat{S} = \frac{\hbar}{2}\widehat{\sigma}$ is the spin vector operator in terms of Pauli matrices $\widehat{\sigma}_x$, $\widehat{\sigma}_y$, $\widehat{\sigma}_z$, $g = 2$ is the g-factor of the electron, and μ_B is the Bohr magneton, respectively [50H1].

When comparing (27.3) with (27.19) we conclude that any TLS is dynamically equivalent to a spin-1/2 system (zero energy such that $\epsilon_2 = -\epsilon_1$). The level-splitting between the ground state and the excited state of the atom corresponds to a constant magnetic field in z-direction, whereas the light field is equivalent to an oscillatory magnetic field in the x-direction. The expectation value of the (pseudo-) spin operator is closely related to the complex dipole moment and the inversion:

$$S_1 = <\widehat{\sigma}_x> = c_1^* c_2 + c_1 c_2^* \quad = 2\,\mathrm{Re}\,\mathcal{P}(t), \tag{27.20}$$

$$S_2 = <\widehat{\sigma}_y> = -ic_1^* c_2 + ic_1 c_2^* = 2\,\mathrm{Im}\,\mathcal{P}(t), \tag{27.21}$$

$$S_3 = <\widehat{\sigma}_z> = \mid c_1 \mid^2 - \mid c_2 \mid^2 \; = -I(t). \tag{27.22}$$

The vector $\boldsymbol{S} = (S_1, S_2, S_3)$ obeys the Bloch equation

$$\frac{\mathrm{d}\boldsymbol{S}(t)}{\mathrm{d}t} = \boldsymbol{\Omega} \times \boldsymbol{S}(t) + \dot{\boldsymbol{S}}_{rel}, \qquad \boldsymbol{\Omega} = (-2\omega_R(t), 0, -\omega_0)\ , \tag{27.23}$$

which describes a rotation of $\boldsymbol{S}$ around a vector $\boldsymbol{\Omega}$ at each instant of time. These equations are identical with the classical equations of motion of a spherical top in an external field (yet with fixed magnitude of the angular momentum) (see Fig. 27.3). The relaxation term $\dot{\boldsymbol{\Omega}}_{sc}$ is of similar structure as (27.17).

In RWA, the rotation vector $\boldsymbol{\Omega} = (-2\omega_R \cos\omega t, 0, -\omega_0)$, is replaced by

$$\boldsymbol{\Omega}_{RWA} = (-\omega_R \cos\omega t, \omega_R \sin\omega t, -\omega_0) \tag{27.24}$$

so that the notation eventually becomes obvious. The linearly polarized electromagnetic wave is decomposed into two counter-rotating circular (pseudo-magnetic) waves and only the resonant component is retained, which rotates with the same chirality as the spin vector.

In the absence of relaxation, the length of the Bloch vector is conserved, $|\boldsymbol{S}| = 1$ [which is equivalent to (27.18)] and its motion can be nicely visualized (see Fig. 27.3). We consider two limiting cases.

- For $\boldsymbol{E}(t) = 0$, $\boldsymbol{S}$ rotates on a cone around the z-axis, which is called the *Larmor precession*

$$\boldsymbol{S}_{\mathrm{L}}(t) = \left(s_0 \sin\omega_0 t, s_0 \cos\omega_0 t, 1 - s_0^2\right), \quad 0 \le |s_0| \le 1. \tag{27.25}$$

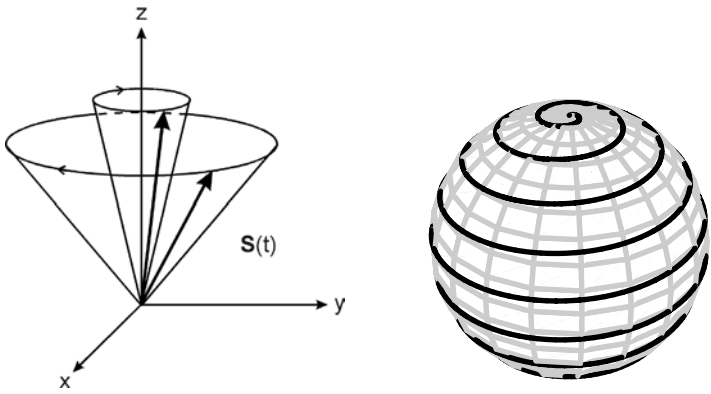

Fig. 27.3. Larmor precession of the Bloch vector in a constant magnetic field $\boldsymbol{B} \parallel z$ (left) and Rabi flopping due to an additional superimposed *ac* field along the 1-direction (right) (without relaxation)

- If the system is excited at a resonance from initial state $\boldsymbol{S}(0) = (0, 0, 1)$ the angle of the Larmor cone increases with time and the Bloch vector performs a spiral motion on the unit sphere from the north to the south pole and vice versa (Rabi flopping). In RWA, we have

$$\boldsymbol{S}_{\mathrm{R}}(t) = (\sin\omega_{\mathrm{R}}t \sin\omega_0 t, \sin\omega_{\mathrm{R}}t \cos\omega_0 t, \cos\omega_{\mathrm{R}}t)\,. \tag{27.26}$$

For Rabi frequencies comparable with or even larger than the atomic transition frequency, the regime of extreme nonlinear optics is reached. Obviously, the two-level approximation is no longer well justified in this regime but, nevertheless, it seems to describe the physics fairly well. For an overview of the amazing complexity and beauty of the nonlinear optical response see Sect. 19.3 and the paper by Tritschler et al. [03T1].

27.1.4 Linear Response of a Two Level System

We are looking for a solution of (27.14,27.15) in a linear approximation with respect to the light field and zero temperature. In this case $I(t) = -1$ in (27.14) so the problem of finding a solution reduces to

$$\left[\frac{\mathrm{d}}{\mathrm{d}t} + (\imath\omega_0 + \gamma)\right] \mathcal{P}(t) = -i\frac{d}{\hbar} E_z(t), \tag{27.27}$$

where $\gamma = 1/T_2$. For $\mathcal{P}(-\infty) = 0$ the solution reads

$$\mathcal{P}(t) = -i\frac{d}{\hbar} \int_{-\infty}^{t} e^{-(\imath\omega_0+\gamma)(t-t')} E_z(t')\,\mathrm{d}t'. \tag{27.28}$$

In particular, for a monochromatic field the dipole moment (27.4) becomes

$$d(t) = \mathrm{Re}\, \alpha(\omega) E_0\, e^{-\imath\omega t}, \tag{27.29}$$

$$\alpha(\omega) = \frac{|d|^2}{\hbar} \left[\frac{1}{\omega_0 - (\omega + \imath\gamma)} + \frac{1}{\omega_0 + (\omega + \imath\gamma)} \right]. \tag{27.30}$$

$\alpha(\omega)$ is the polarizability of the TLS. Remarkably, this result is almost identical with the polarizability of a classical harmonic oscillator (e.g., a particle with mass m and charge e bound to a spring with $D = m\,\omega_0^2$, see Chap. 4).

$$\alpha_{cl}(\omega) = \frac{\frac{e^2}{m}}{\omega_0^2 - \omega^2 - 2\imath\gamma\omega} \tag{27.31}$$

In contrast to (27.30), the resonance frequency of a classical oscillator shifts with increasing damping to lower values $\sqrt{\omega_0^2 - \gamma_2^2}$.

27.2 Optical Bloch Equations

As sketched in Fig. 27.4 the generalization of the optical Bloch equations to the case of a two-band semiconductor is straightforward. Neglecting the momentum of the absorbed photon, the optical transitions are vertical in $\boldsymbol{k}$-space. Under homogeneous conditions and neglect of scattering processes (between different $\boldsymbol{k}$-states in the same band) a two-band semiconductor is just an assembly of uncoupled TLSs and resembles the case of a inhomo-

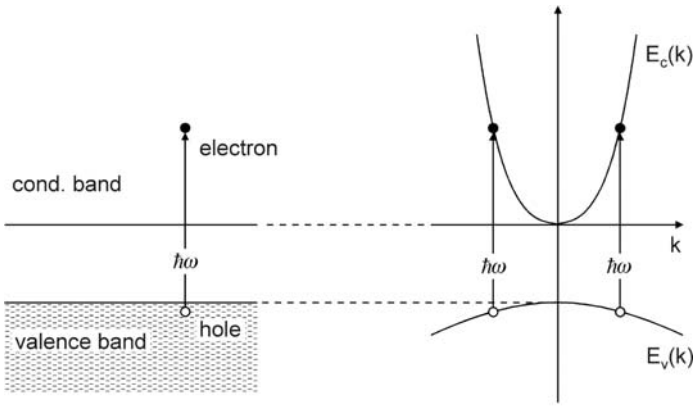

Fig. 27.4. Two noninteracting bands viewed as a collection of TLSs with different transition energies

geneously broadened line problem in atomic physics. The equations of motion are:

$$i\hbar\frac{\partial\mathcal{P}(\boldsymbol{k},t)}{\partial t} = \Big[E_c(\boldsymbol{k}) - E_v(\boldsymbol{k})\Big]\mathcal{P}(\boldsymbol{k},t) + \boldsymbol{d}_{cv}(\boldsymbol{k})\boldsymbol{E}(t)\Big[n_c(\boldsymbol{k},t) - n_v(\boldsymbol{k},t)\Big] + i\hbar\dot{\mathcal{P}}_{rel}, \tag{27.32}$$

$$\frac{\partial n_c(\boldsymbol{k},t)}{\partial t} = -\,2\,\mathrm{Im}\,\Big[\boldsymbol{d}_{cv}(\boldsymbol{k})\boldsymbol{E}(t)\mathcal{P}^*(\boldsymbol{k},t)\Big] + \dot{n}_c^{rel}, \tag{27.33}$$

$$\frac{\partial n_v(\boldsymbol{k},t)}{\partial t} = +\,2\,\mathrm{Im}\,\Big[\boldsymbol{d}_{cv}(\boldsymbol{k})\boldsymbol{E}(t)\mathcal{P}^*(\boldsymbol{k},t)\Big] + \dot{n}_v^{rel}. \tag{27.34}$$

These are the optical Bloch equations. n_c and n_v are the mean occupation numbers (per spin) of the conduction and valence band Bloch states. In addition, particle conservation requires $n_c + n_v = 1$. In a phenomenological description, relaxation may be included analogously to (27.17). For a qualitative treatment and allowed (dipole) transitions, the $\boldsymbol{k}$-dependence of the interband dipole matrix element $\boldsymbol{d}_{\mathrm{cv}}(\boldsymbol{k}) \propto \langle c, \boldsymbol{k}\,|\widehat{\boldsymbol{p}}|\,v, \boldsymbol{k}\,\rangle$ may often be neglected near the band edge. The $\boldsymbol{k}$-dependence is only relevant for forbidden transitions or if the variation of the polarization over the whole Brillouin-zone is needed. Note that these equations are uncoupled with respect to the wave number $\boldsymbol{k}$.

From $\mathcal{P}(\boldsymbol{k},t)$ the electronic polarization of the semiconductor can be obtained from

$$\boldsymbol{P}(t) = \frac{2}{V}\,\mathrm{Re}\sum_{\boldsymbol{k},s}\boldsymbol{d}_{cv}^*(\boldsymbol{k})\,\mathcal{P}(\boldsymbol{k},t), \tag{27.35}$$

where V denotes volume of the sample, which eventually drops out when performing the sum over wavenumbers in terms of the integral

$$\frac{1}{V}\sum_{\boldsymbol{k},s}\ldots = 2\frac{1}{(2\pi)^d}\int\ldots d^d\boldsymbol{k}, \tag{27.36}$$

where $d = 1, 2, 3$ specifies the space-dimension and the factor 2 arises from spin summation.

27.2.1 Optical Susceptibility: Interband Transitions

Next, we discuss the linear response result for the optical susceptibility of an undoped semiconductor at low temperatures and neglecting crystal anisotropy. Here, n_c and n_v can be replaced by the (equilibrium) Fermi functions $f_c(k) \approx 0$, $f_v(k) \approx 1$ for the electrons in the conduction and valence bands. As $\boldsymbol{k}$ is merely a parameter in this approximation, the required solution of (27.32) can be found by the ansatz

$$\mathcal{P}(\boldsymbol{k},t) = Q(\boldsymbol{k},t)\exp\Big[-\frac{i}{\hbar}\left(E_c(\boldsymbol{k}) - E_v(\boldsymbol{k})\right)t\Big] \tag{27.37}$$

with a simple integration of $Q(\boldsymbol{k},t)$. Eventually, we read off the electrical susceptibility $\chi(\omega)$ from the Fourier components of $\boldsymbol{P}(t)$ and $\boldsymbol{E}(t)$ (see Prob. 3):

$$\boldsymbol{P}(\omega) = \epsilon_0 \chi(\omega)\, \boldsymbol{E}(\omega), \tag{27.38}$$

$$\chi(\omega) = \frac{1}{V\epsilon_0} \sum_{k,s} |d_{cv}(\boldsymbol{k})|^2 \left\{ \frac{f_v(\boldsymbol{k}) - f_c(\boldsymbol{k})}{E_c(\boldsymbol{k}) - E_v(\boldsymbol{k}) - \hbar(\omega + i\eta)} + \right.$$
$$\left. + \frac{f_v(\boldsymbol{k}) - f_c(\boldsymbol{k})}{E_c(\boldsymbol{k}) - E_v(\boldsymbol{k}) + \hbar(\omega + i\eta)} \right\}, \quad \eta \to +0. \tag{27.39}$$

For parabolic bands and $\boldsymbol{k}$-independent dipole matrix elements d_{cv} (along the field direction) the absorptive part of the susceptibility is proportional to the joint density of states of the valence and conduction bands. In the $d = 1, 2, 3$ dimensions, the (joint) density of states, and hence the absorption, rises as $\mathrm{Im}\ \chi(\omega) \propto [\hbar\omega - E_g]^{(d-2)/2}$ (see also Sect. 7.7 and 8.9).

27.3 Semiconductor Bloch Equations

We are close to the summit of our tour towards SBEs. Two features have not yet been taken into account:

- There is a change in Coulomb and exchange energy of the interacting many-electron (ground) state when exciting an electron to the conduction band and leaving a hole behind. The main part of this interaction turns out to be an attractive Coulomb potential, which adds to the external electrical field (also see Chap. 9).
- With increasing band filling there is a renormalization of the electron/hole band energy by the electron/hole Coulomb interaction (also see Chap. 21).

$$i\hbar \frac{\partial \mathcal{P}(\boldsymbol{k},t)}{\partial t} = \Big[E_g + E_e(\boldsymbol{k}) + E_h(\boldsymbol{k}) \Big] \mathcal{P}(\boldsymbol{k},t)$$
$$+ \Big[n_e(\boldsymbol{k},t) + n_h(\boldsymbol{k},t) - 1 \Big] \hbar\Omega_{\mathrm{R}}(\boldsymbol{k},t) + i\hbar \dot{\mathcal{P}}_{rel}, \tag{27.40}$$

$$\frac{\partial n_c(\boldsymbol{k},t)}{\partial t} = -2\,\mathrm{Im} \left\{ \Omega_{\mathrm{R}} \mathcal{P}^*(\boldsymbol{k},t) \right\} + \dot{n}_c^{rel}, \tag{27.41}$$

$$\frac{\partial n_h(\boldsymbol{k},t)}{\partial t} = -2\,\mathrm{Im} \left\{ \Omega_{\mathrm{R}} \mathcal{P}^*(\boldsymbol{k},t) \right\} + \dot{n}_h^{rel} \tag{27.42}$$

For convenience, the change in population of the valence band is formulated within the hole picture (as indicated by the index h):

$$n_v(\boldsymbol{k},t) = 1 - n_h(\boldsymbol{k},t), \qquad E_v(\boldsymbol{k},t) = -E_g - E_h(\boldsymbol{k},t). \tag{27.43}$$

The factor $n_e(\boldsymbol{k},t) + n_h(\boldsymbol{k},t) - 1$ is again the population inversion at $\boldsymbol{k}$. Its influence on the optical absorption is often denoted as phase space filling or

Pauli-blocking. The term $-2\mathrm{Im}\{\Omega_R \mathcal{P}^*(\boldsymbol{k},t)\}$ in (27.41, 27.42) describes the generation of electron hole pairs by the absorption of light.

$E_e(\boldsymbol{k},t)$ and $E_h(\boldsymbol{k},t)$ are the electron/hole (Hartree-Fock) energies including the interaction with other electrons/holes. For parabolic bands these are:

$$E_j(\boldsymbol{k},t) = \frac{\hbar^2 \boldsymbol{k}^2}{2m_j} - \frac{1}{V} \sum_{\boldsymbol{q}\ (\neq \boldsymbol{k})} V(\boldsymbol{k}-\boldsymbol{q})\, n_j(\boldsymbol{q},t), \quad j = e,h. \tag{27.44}$$

Note, $m_h > 0$.

$\Omega_{\mathrm{R}}(\boldsymbol{k},t)$ denotes the generalized Rabi frequency (function)

$$\hbar\Omega_{\mathrm{R}}(\boldsymbol{k},t) = \boldsymbol{d}_{\mathrm{cv}}(\boldsymbol{k})\boldsymbol{E}(t) + \frac{1}{V} \sum_{\boldsymbol{q}\ (\neq \boldsymbol{k})} V(\boldsymbol{k}-\boldsymbol{q})\, \mathcal{P}(\boldsymbol{q},t), \tag{27.45}$$

where $V(\boldsymbol{q})$ is the Fourier transform of the (repulsive) Coulomb potential screened by a background dielectric constant ϵ_b

$$V(\boldsymbol{q}) = \frac{e^2}{\epsilon_0 \epsilon_b\, q^2}, \qquad V(\boldsymbol{r}) = \frac{e^2}{4\pi\epsilon_0 \epsilon_b\, r}. \tag{27.46}$$

Going beyond the time-dependent Hartree-Fock approximation is not easy and requires higher-order correlation functions. Physically, this leads to a further renormalization of interactions and energies, which are described by four, six, or more particle (e.g., biexcitons) amplitudes, and a microscopic formulation of the relaxation terms (dephasing of the polarization, collisions of electrons and holes) [88Z1, 94H1, 96H1]. An important mechanism in this respect is the dynamical screening of the (e–e, h–h, e–h) Coulomb interactions by the excited carriers in terms of a (Lindhard-) dielectric function $\epsilon_\ell(\boldsymbol{q},\omega)$. Such contributions are of increasing importance for high excitation and ultrashort pulses. Moreover, in addition to the purely electronic interactions there are other scattering mechanisms, such as carrier-phonon scattering or scattering of the carriers by impurities and interface roughness in spatially confined systems. For very short times, memory effects of the scattering processes come into play so that the scattering integrals in the Boltzmann equation for n_e, n_h become non-Markovian.

Further refinements of the theory may also include some details of the realistic semiconductor band-structure (e.g., more than two bands, heavy hole-light hole splitting, band-warping, etc.) or spatial dispersion. This, however, requires a huge numerical effort. At this level one is generally left with an approximate numerical treatment and the problem is considered to be understood (or solved) if these results agree well with the experimental findings.

27.3.1 Optical Susceptibility: Excitons

To demonstrate the simplicity as well as the potential of SBEs (e.g., as compared with Elliott's evaluation of the Kubo formula [57E1]) we discuss the

linear optical susceptibility of the interacting electron-hole system including exciton states. At low excitation and zero temperature we have $n_v = n_h \approx 0$ so that (27.40-27.42) reduce to:

$$i\hbar\frac{\partial\mathcal{P}(\boldsymbol{k},t)}{\partial t} = \Big[E_g + \frac{\hbar^2\boldsymbol{k}^2}{2\mu_r}\Big]\mathcal{P}(\boldsymbol{k},t) - \frac{1}{V}\sum_{q(\neq\boldsymbol{k})} V(\boldsymbol{k}-\boldsymbol{q})\mathcal{P}(\boldsymbol{q},t) - \boldsymbol{d}_{cv}\boldsymbol{E}(t). \quad (27.47)$$

μ_r denotes the reduced electron hole mass. As opposed to the optical Bloch equations, (27.32-27.34), $\boldsymbol{k}$ is no longer just a parameter; different $\boldsymbol{k}$s are coupled by $V(\boldsymbol{k}-\boldsymbol{q})$. However, this interaction term is a convolution type and, by Fourier-transformation, it reveals as the (inhomogeneous) Schrödinger equation of the hydrogen atom

$$i\hbar\frac{\partial\mathcal{P}(\boldsymbol{r},t)}{\partial t} = \Big[E_g - \frac{\hbar^2}{2\mu_r}\Delta\Big]\mathcal{P}(\boldsymbol{r},t) - V(\boldsymbol{r})\mathcal{P}(\boldsymbol{r},t) - \boldsymbol{d}_{cv}\,\boldsymbol{E}(t)\,\delta(\boldsymbol{r}). \quad (27.48)$$

Equation (27.48) is also known as the Wannier-Equation. $\mathcal{P}(\boldsymbol{r},t)$ plays the part of the exciton (envelope) wave function. The $\boldsymbol{k}$-dependence of the interband matrix element $\boldsymbol{d}_{cv}(\boldsymbol{k})$ has been neglected.

For $\boldsymbol{E} = 0$ the stationary states are well known from standard texts on quantum mechanics

$$\mathcal{P}_\alpha(\boldsymbol{r},t) = e^{-i\frac{E_\alpha}{\hbar}t}\,\Psi_\alpha(\boldsymbol{r}), \quad E_\alpha = -\frac{Ry^*}{n^2}, \quad Ry^* = Ry\,\frac{\mu_r/m_0}{\epsilon_b^2}. \quad (27.49)$$

Ry $= 13.6\ldots$ eV is the hydrogenic Rydberg energy.[5] Quantum numbers $\alpha = (n,l,m)$ have their usual meaning and, formally, n labels the discrete, as well as the continuum, states. In a semiconductor, these (bound) hydrogenic states are called *excitons*, which have been extensively discussed in previous chapters, (in particular see Chaps. 9, 13 and the references cited therein).

For $\boldsymbol{E}(t) \neq 0$ (parallel to the z-direction) we seek the solution of $\mathcal{P}(\boldsymbol{r},t)$ in terms of the complete set of the stationary states as given by (27.49),

$$\mathcal{P}(\boldsymbol{r},t) = \sum_\alpha Q_\alpha(t)\mathcal{P}_\alpha(\boldsymbol{r},t), \quad (27.50)$$

where $Q_\alpha(t)$ can be found by the simple integration

$$Q_\alpha(t) = i\frac{d_{\rm cv}}{\hbar}\Psi^*_\alpha(\boldsymbol{r}=0)\int_{-\infty}^{t} E_z(t')\,e^{i\frac{E_\alpha}{\hbar}t'}e^{\eta t'}\,{\rm d}t', \quad \eta\to 0^+. \quad (27.51)$$

$\exp(\eta t)$ has been added to switch on the light at $t=-\infty$ adiabatically. Obviously, the (spatially constant) light-field creates only those exciton states that have a nonvanishing wave function at the origin; these are the s-states.[6]

[5] If the excitonic Rydberg Ry* is smaller than the LO-phonon energy, ϵ_b is given by the static dielectric constant ϵ_s and otherwise by ϵ_∞ (see also Sect. 9.2).

[6] This result originates from our approximation that $\boldsymbol{d}_{\rm cv}(\boldsymbol{k}) = {\rm const}$. If the dipole element vanishes linearly with $\boldsymbol{k}$ at the band edge, the coupling is solely to p-states. A prominent example is Cu_2O (see Sect. 13.2.1.2 and Prob. 4.)

Inserting (27.50) in (27.36) and using the completeness relation of the stationary states (27.49), we finally obtain the electrical susceptibility (isotropic approximation, $d_{\rm cv}$ along $\boldsymbol{E}$)

$$\chi(\omega) = 2\frac{|d_{\rm cv}|^2}{\epsilon_0} \sum_\alpha |\Psi_\alpha(\boldsymbol{r}=0)|^2 \left\{ \frac{1}{E_g + E_\alpha - \hbar(\omega + i\eta)} + \right.$$
$$\left. + \frac{1}{E_g + E_\alpha + \hbar(\omega + i\eta)} \right\}. \tag{27.52}$$

In a bulk semiconductor the absorptive part consists of a series of delta-functions at the bound exciton s-states with rapidly decreasing oscillator strength $\propto n^{-3}$ and a continuum part [94H1]

$$\text{Im } \chi(\omega) \propto \sum_{n=1}^{\infty} \frac{4\pi}{n^3} \delta(\Delta + \frac{1}{n^2}) + \theta(\Delta) \frac{\pi \exp\left(\frac{\pi}{\sqrt{\Delta}}\right)}{\sinh(\frac{\pi}{\sqrt{\Delta}})}. \tag{27.53}$$

$\Delta = (\hbar\omega - E_g)/\text{Ry}^*$ denotes the normalized photon energy. Close to the ionization continuum, $\Delta \to 0$, the absorption increases stepwise in striking distinction to the square root law for noninteracting bands (cf. (27.39)). Thus, the attractive Coulomb interaction not only creates bound states below the gap but leads to a pronounced enhancement of the absorption above the gap (the so-called Sommerfeld-enhancement). Equation (27.53) was first derived by Elliott [57E1] but in a much more elaborate way. The corresponding real part can be calculated from the Kramers–Kronig relations (see Chap. 6).

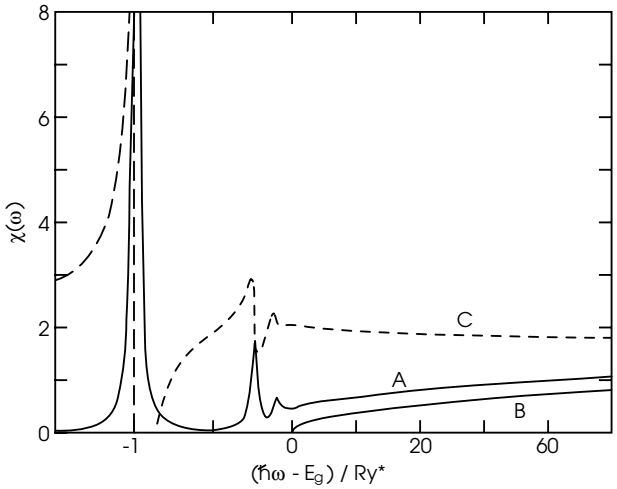

Fig. 27.5. Electrical susceptibility of a direct semiconductor near the gap energy. Im χ (A) and Re χ (B) of the interacting electron hole system, (27.53). Im χ (B) of the noninteracting system, (27.39). Note the different frequency scale above and below the gap. An appropriate broadening was included phenomenologically [87S1]

The optical absorption spectrum bulk GaAs is displayed in Fig. 27.5, which gives a lively impression of the importance of the Coulomb interaction and exciton states near the band gap. In the very best samples, exciton lines up to $n = 3$ can be resolved in this material (see Chap. 13).

27.4 Some Selected Coherent Processes

An important class of optical experiments involves two or three short pulses impinging from different directions and at different times on the sample (see Fig. 27.6 and Sects. 23.2.1.1 and 25.2.2.3). From the analysis of such studies on the dynamics and coherence properties, such as T_1, the T_2 times are obtained. In terms of nonlinear optics, the processes in question are of third order with respect to the light

$$P_j = \chi^{(3)}_{jklm} E_k E_l E_m . \tag{27.54}$$

The products are in fact convolutions with respect to time, and j, k, l, m denote Cartesian components of the (total) electrical light field. One of these pulses, shown in Fig. 27.6, may have a twofold effect. The following sections discuss some typical examples.

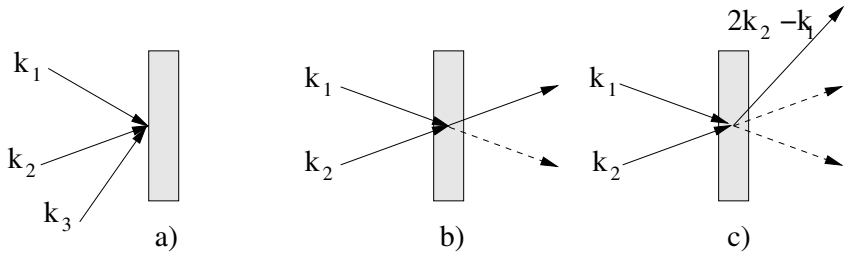

Fig. 27.6. (**a**) Sketch of some third-order nonlinear processes. (**b**) Pump-probe (**c**) Four-wave mixing experiment

27.4.1 Pump-Probe Experiments

In a pump-probe experiment the first pulse (pump) pre-excites the system. After a delay time τ the linear optical (absorption, reflection) response with a second pulse (probe) is measured. As a reference, we give the result for the optical Bloch equations, where a $\delta(t)$ shaped pulse #1 induces the following change in the optical absorption

$$\delta\alpha(\omega;\tau,I_1) = \alpha(\omega;\tau,I_1) - \alpha_0(\omega) \propto -I_1\, e^{\tau/T_1}\, \alpha_0(\omega)\,. \tag{27.55}$$

Hence, pump-probe experiments reflect the influence of the excited carriers and their relaxation on the optical properties. $\alpha_0(\omega)$ is the absorption coefficient of the system in equilibrium. In Fig. 27.6b the electrical field of pulse #1 enters twice because $I_1 \propto E_1^2$.

27.4.2 Four-Wave Mixing Experiments

In a wave mixing experiment the nonlinear response is studied in a so-called background free direction, which is different from those of the incident pulses and their transmission or reflection, which, of course, is experimentally favorable (see also Chap. 25). The first pulse excites a coherent polarization whose radiation field interferes with the second pulse forming an interference pattern with wave vector $\boldsymbol{k}_1 - \boldsymbol{k}_2$. This pattern, in turn, modulates the (linear) optical properties of the system and, thus, diffracts off the second pulse in direction $2\boldsymbol{k}_2 - \boldsymbol{k}_1$ (other directions are less efficient). This phenomenon is called (degenerate) four-wave mixing (FWM) as four waves are involved: #1, #2 (counted twice!) and the wave emitted in the direction $2\boldsymbol{k}_2 - \boldsymbol{k}_1$ (see Fig. 27.6c).

For a general overview of nonlinear coherent processes in semiconductors, see Haug and Koch [94H1], Shah [96S1], or Schäfer and Wegener [02S1]. A review on the coherent spectroscopy of semiconductor microcavities has been given by Lyssenko et al. [05L1]. Experimental results for typical semiconductor systems are discussed in Chap. 23.

27.4.3 Photon Echo

The analogy of a TLS with the spin-1/2 problem offers an unexpected insight into an interesting phenomenon called *photon echo*. Here, we examine the rather marvelous notion that not all macroscopic decay processes are irreversible.[7] In a photon echo experiment, many TLS are usually involved and because of different local environments these have individually slightly different transition frequencies (inhomogeneous line broadening, spectral width parameterized by $1/T_2^*$). Hence, the macroscopic (magnetization or polarization) signal contains many contributions with slightly different frequencies that add up almost to zero in a rather short time ($\approx T_2^*$), yet the individual systems are still oscillating with a fixed phase relation with respect to the exciting pulse and the energy stored in the moments being out of phase can be recovered in a coherent fashion. Instead of waiting for the extremely unlikely Poincaré recurrence of the initial state, a second pulse after time T is used, which – loosely speaking – causes a time reversal operation followed by an echo of the initial pulse after total time $2T$.

[7] This technique was developed by Hahn [50H1] for nuclear spin systems and it plays an important role in measuring the T_2-time. For a survey and thorough discussion we refer readers to Chap. 9 of Allen and Eberly [87A1] and to Chap. 23 of this book for experimental results.

To uncover the echo phenomenon it is convenient to describe the dynamics of the Bloch vector in a frame rotating with the frequency of the light (not the atomic transition frequency!) around the 3-axis:

$$R_1(t) = S_1(t)\cos\omega t - S_2(t)\sin\omega t, \tag{27.56}$$
$$R_2(t) = S_1(t)\sin\omega t + S_2(t)\cos\omega t, \tag{27.57}$$
$$R_3(t) = S_3(t). \tag{27.58}$$

(In complex notation the $1,2$ components can be summarized by $R = R_1 + iR_2$, $S = S_1 + iS_2$, with $R = Se^{i\omega t}$.) In this frame the equations of motion read

$$\dot{R}_1(t) = -\delta R_2(t) - \frac{R_1(t)}{T_2}, \tag{27.59}$$
$$\dot{R}_2(t) = +\delta R_1(t) + \omega_R R_3(t) - \frac{R_2(t)}{T_2}, \tag{27.60}$$
$$\dot{R}_3(t) = -\omega_R R_2(t) - \frac{R_3(t) - R_3^{eq}}{T_1}. \tag{27.61}$$

These linear differential equations have constant coefficients so that the solution can be found by an exponential ansatz. In particular, for $\omega_R = 0$ the Bloch vector performs a (damped) Larmor-precession around the 3-axis:

$$R_1(t) = [R_1(0)\cos\delta t - R_2(0)\sin\delta t]\; e^{-\frac{t}{T_2}}, \tag{27.62}$$
$$R_2(t) = [R_1(0)\sin\delta t + R_2(0)\cos\delta t]\; e^{-\frac{t}{T_2}}, \tag{27.63}$$
$$R_3(t) = R_3^{eq} + [R_3(0) - R_3^{eq}]\; e^{-\frac{t}{T_1}}. \tag{27.64}$$

At resonance, $\delta = 0$, but by neglecting damping a light pulse causes a Rabi rotation of the Bloch vector around the 1-axis

$$R_1(t) = +R_1(0), \tag{27.65}$$
$$R_2(t) = +R_2(0)\cos\omega_R t + R_3(0)\sin\omega_R t, \tag{27.66}$$
$$R_3(t) = -R_2(0)\sin\omega_R t + R_3(0)\cos\omega_R t. \tag{27.67}$$

In the discussion of a photon echo experiment four periods have to be distinguished (see Fig. (27.7)). To simplify matters, we shall assume that the pulse duration is short with respect to T_1, T_2, T_2^* and intense, $\omega_R T_2^* \gg 1$, so that the influence of damping and detuning can be safely neglected during the pulses.

1. All TLSs start from the same initial state $\mathbf{R}^{(0)} = (0,0,1)$. Then the ensemble of atoms is polarized by an initial light pulse (duration τ_1), which, according to (27.65–27.67), leads to a common Bloch vector $\mathbf{R}^{(1)} = (u,v,w)$. For a so-called $\pi/2$-pulse, i.e., $\phi_1 = \omega_R\tau_1 = \pi/2$, the polarization (magnetization) is "tipped" to the 2-direction: $\mathbf{R}^{(1)} = (0,1,0)$ (see Fig. 27.7a).
2. After the first light pulse, the individual Bloch vectors $\mathbf{R}^{(2)}$ precess according to (27.62–27.64). Because of their slightly different frequencies the individual dipole moments get out of phase (relative to each other) and

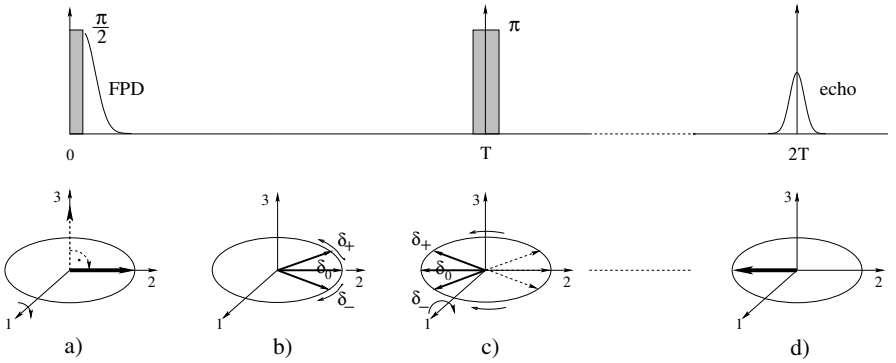

Fig. 27.7. Principle of a photon echo experiment. *Upper part*: Standard pulse sequence (*dashed blocks*, exaggerated duration) and resulting polarization (*solid lines*). *Lower part*: Dynamics of the Bloch vector in the rotating frame. (**a**) Alignment of the individual Bloch vectors along the 2-direction by a $\pi/2$-rotation around the 1-axis. (**b**) Precession of the individual Bloch vectors in the 1-2 plane as determined by their various detunings leading to free polarization decay (FPD). (**c**) π-rotation around the 1-axis transforms $R_2 \to -R_2$ but leaves R_1 unchanged. (**d**) Reproduction of the initial state at time T after the π-pulse (For simplicity only three Bloch vectors are displayed with detunings $\delta_+ > 0$, $\delta_0 = 0$, $\delta_- < 0$)

add to zero in a time T_2^*, which is much shorter than T_2. This dephasing phenomenon is called *free polarization decay* (FPD) and is depicted in Fig. 27.7b. (Since we are in a rotating frame only the phase deviations relative to $\exp(i\omega t)$ appear in this figure.)

3. After time T a second light pulse is applied (duration τ_2, phase $\phi_2 = \omega_R \tau_2$), which, according to (27.65, 27.66), tips the polarization to $\mathbf{R}^{(3)}$.
4. After the second pulse the Bloch vectors $\mathbf{R}^{(4)}$ again rotate freely around the 3-axis. As a result, we obtain for the 2-component

$$R_2^{(4)}(t) = \Big\{ u\left[\cos\delta T \sin\delta t + \cos\phi_2 \sin\delta T \cos\delta t\right] \tag{27.68}$$

$$-v\left[\sin\delta T \sin\delta t - \cos\phi_2 \cos\delta T \cos\delta t\right] \Big\} e^{-\frac{t+T}{T_2}} \tag{27.69}$$

$$+ \sin\phi_2 \cos\delta t \left[1 + (w-1)\, e^{-T/T_1}\right] e^{-T/T_2}, \tag{27.70}$$

where the time t counts from the end of the second pulse. For $\phi_2 = \pi$ the terms in the [..] brackets combine to $\cos\delta(T-t)$ and $\sin\delta(T-t)$ and all individual Bloch vectors are again in phase at time $2T$ after the first pulse and add up to a macroscopic polarization. This causes the emission of a light pulse, the photon echo.

The resurrected free polarization signal has the magic quality of something coming from nothing. However, this resurrection is only possible for times comparable with the T_2 time. For larger times, the intensity of the photon

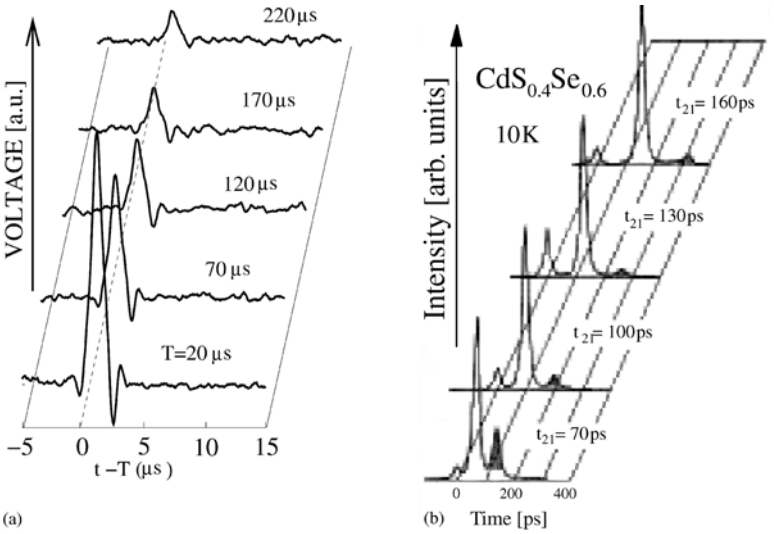

Fig. 27.8. Experimental spin echo for protons in water ($\omega/2\pi = 95$MHz, duration of π-pulse: 1.4μs, $T_2 \approx 75\mu$s, $T_2^* \approx 1\mu$s, $T_1 \approx 10$s, room temperature) [03F1] (*left*) and photon echo in a II-VI semiconductor compound [92S1](*right*)

echo decays as the square of $\exp(-2T/T_2)$, i.e., $\exp(-4T/T_2)$. T_2 is also called the *decoherence or dephasing time*.

It is interesting that the existence of the echo is not attributed to the π-character of the second pulse as it is frequently imputed. When decomposing the products of trigonometric functions $\cos\delta T \cos\delta t$, etc., in terms of sum and differences, we realize that there is a contribution to the polarization of the form:

$$R_2^{(4)} = -\frac{1-\cos\phi_2}{2}\Big\{u\sin\left[\delta(T-t)\right] + v\cos\left[\delta(T-t)\right]\Big\}e^{-\frac{t+T}{T_2}} + \ldots \quad (27.71)$$

Thus, a second pulse of *any duration* will induce an echo. However, its intensity is largest for $\phi_2 = \pi$ (and $\phi_1 = \pi/2$). (Terms omitted in (27.71) indicate nonecho terms).

Although spin and photon echo phenomena have the same theoretical roots, there are profound experimental differences.

- In semiconductors, photon echoes are generated with light pulses that correspond to phase shifts much smaller than π. $\Phi = \pi$ would lead to a complete band inversion, which in turn would lead to a collapse of the semiconductor band structure. This regime is hardly accessible and would generate additional fast dephasing processes.
- Spin echoes are generated with rf or microwave fields with wavelengths much larger than the dimensions of the specimen. The situation is opposite for photon echoes in semiconductors where standard experimental

techniques, e.g., four-wave mixing, uses pulses traveling in different directions so that the echo signal can be spatially separated from the exciting pulses (details are discussed in Chaps. 23 and 25).

A popular analogy of the spin echo phenomenon and a group of runners in a stadium as discussed in Chap. 9 of Allen and Eberly's book [87A1] and in Sect. 23.2 of this book. (However, it should be kept in mind that π-rotation around the 1-axis at time T causes a reconfiguration of the pulse, analogously to optical phase conjugation, rather than a reversal of time of the individual Bloch vectors.)

Experimentally, photon echo measurements are often used as a tool to determine the optical dephasing rate T_2^{-1}. In semiconductor systems, however, the (dynamically screened) interactions of the electron hole pairs may lead to significant deviations from the atomic case and the analysis of experimental results requires a detailed numerical study of the SBEs, which was first undertaken by Lindberg et al. [92L1]. For an overview and details see Haug and Koch [94H1] and Schäfer and Wegener [02S1]. An easily readable review of spin echo and photon echo in semiconductors, as well as an overview on related echo phenomena, was recently published by Meier and Thomas [03M1].

A preliminary version of this chapter was published in the proceedings of an Erice Summer School [98B1].

27.5 Problems

1. Solve (27.12) for arbitrary detuning and calculate the wave function coefficients $c_j(t)$ (or $a_j(t)$), inversion $I(t)$, and complex polarization $\mathcal{P}(t)$. Use the initial conditions $c_1(0) = 1$ and $c_2(0) = 0$.
2. At resonance there are stationary states of the coupled TLS electrical field, (27.12), with time-independent probabilities $|c_j(t)|^2$=const. Find these "dynamic Stark-states."
3. Use the ansatz proposed by (27.37) to solve (27.32) for a monochromatic field and derive the interband susceptibility $\chi(\omega)$ given by (27.39). Hint: In the absence of damping, the light field must be switched on adiabatically at $t = -\infty$, $\boldsymbol{E}(t) = E_0 \exp(\eta t) \cos(\omega t)$, $\eta \to +0$. Otherwise the response contains spurious contributions from the physically irrelevant initial state.
4. If the transitions near the band-edge are forbidden (in first order) the dipole matrix element behaves as $\boldsymbol{d}_{cv}(\boldsymbol{k}) \propto \boldsymbol{k}$. Show that the optical absorption is now linked to exciton p-states.
   Hints: For $r \to 0$ hydrogenic wave functions behave as $\Psi_{n,l,m}(r, \theta, \phi) \propto r^l$. Under Fourier transformation: grad $\to \imath \boldsymbol{k}$.
5. Find the general solution of the Bloch equations for the photon echo problem (27.59–27.61). Express the integration constants in terms of the Bloch vector at $t = 0$, $\mathbf{R}(0)$.
   Hint: The solution can be obtained by an exponential ansatz with $\mathbf{R}(t) = \boldsymbol{\rho} \exp(\lambda t)$, where $\boldsymbol{\rho}$ is a time-independent 3-component vector.

6. Consider a photon echo with pulses of equal duration, i.e. $\Phi = \Phi_1 = \Phi_2$. Show that the echo signal has a maximum for $\Phi = 2\pi/3$ and even a bit stronger than that for the $\pi/2$-π sequence.

References to Chap. 27

[46B1] F. Bloch, Phys. Rev. **70**, 460 and 474 (1946).

[50H1] E. L. Hahn, Phys. Rev. **80**, 580 (1950).
See also: *Nonlinear Spectroscopy of Solids, Advances and Applications*, B. Di Bartolo ed., Nato ASI Series B, Vol. 339, page 75 (Plenum, New York and London 1994).

[57E1] R. J. Elliott, Phys. Rev. **108**, 1384 (1957). See also: *Polarons and Excitons*, edited by C. G. Kuper and G. D. Whitfield (Oliver and Boyd, Edinburgh and London 1963).

[64F1] R. P. Feynman, R. B. Leighton, M. Sands, *The Feynman Lectures on Physics*, Vol. III (Addison-Wesley, Reading, Massachusetts, Palo Alto, London 1964).

[70H1] H. Haken, Handbuch der Physik, S. Flügge ed., Vol. XXV/2c, *Light and Matter 1c* (Springer, Berlin, Heidelberg, New York 1970).

[79H1] H. Haken, *Licht und Materie*, Vol. 2 (Bibliographisches Institut, Mannheim, Wien, Zürich 1979).

[84S1] A. Stahl, Solid State Commun. **49**, 91 (1984).

[87A1] L. Allen, J. H. Eberly, *Optical Resonance and Two-Level Atoms* (Dover, New York 1987).

[87S1] A. Stahl, I. Balslev, *Electrodynamics of the Semiconductor Band Edge*, Springer Tracts in Modern Physics, Vol.110 (Springer, Berlin 1987).

[88Z1] R. Zimmermann, *Many Particle Theory of Highly Excited Semiconductors*, (Teubner, Leipzig 1988).

[92B1] R. W. Boyd, *Nonlinear Optics* (Academic Press, Boston 1992).

[92L1] M. Lindberg, R. Binder, S. W. Koch, Phys. Rev. A **45**, 1865 (1992).

[92S1] U. Siegner, D. Weber, E. O. Göbel, D. Bennhardt, V. Heukeroth, R. Saleh, S. D. Baranovskii, P. Thomas, H. Schwab, C. Klingshirn, J. M. Hvam, V. G. Lyssenko, Phys. Rev. **B** 46, 4564 (1992).

[94H1] H. Haug, S. W. Koch, *Quantum Theory of the Optical and Electronic Processes of Semiconductors* (World Scientific, Singapore, New Jersey, London, Hong Kong 1994).

[96H1] H. Haug, A-P. Jauho, *Quantum Kinetics in Transport and Optics of Semiconductors* (Springer, Berlin, Heidelberg 1996).

[96S1] J. Shah, *Ultrafast Spectroscopy of Semiconductor and Semiconductor Nanostructures*, Springer Series in Solid State Sciences, **115**, (1996).

[98B1] R. v. Baltz, in: *Ultrafast Dynamics of Quantum Systems: Physical Processes and Spectroscopic Techniques*, B. Di Bartolo ed., Nato ASI series B, Vol. 372 (Plenum, New York and London 1998).

[02S1] W. Schäfer, M. Wegener, *Semiconductor Optics and Transport Phenomena*, Advanced Texts in Physics (Springer, Berlin 2002).

[03F1] F. Fujara, Ch. Köhler, private communication. Institut für Festkörperphysik, Technische Universität Darmstadt.

[03M1] T. Meier, P. Thomas, *Echoes in Festkörpern*, Physik Journal, März issue, p 53, Wiley-VCH (2003).
[03T1] T. Tritschler, O. D. Mücke, M. Wegener, Phys. Rev. A **68**, 33404 (2003).
[05B1] B. Di Bartolo, in: *Investigating Extreme Physical Conditions with Advanced Optical Techniques*, B. Di Bartolo ed., Nato ASI series II (Kluwer, Dordrecht, Boston, London, to be published).
[05L1] V. Lyssenko, D. Meinhold, B. Rosam, K. Leo, D. Birkedal, J. Erland, M. van der Poel, J. Hvam, *Coherent Spectroscopy of Semiconductor Microcavities*, in Ref. [05B1].

The final problem

Find all errors in this book both in physics and in printing, collect all aspects which can be improved and all important phenomena which have been omitted and solve all problems. Send a corresponding listing to the author and help him by doing so to improve the next editions of this book – if there are any. Many thank inadvance for your help.

Actually, the author himself is working hard on parts of this problem, trying to reduce the number of mistakes and misprints from one edition to the next, but possibly introducing some new ones at the same time. A dear colleague, Prof. Dr. B. Di Bartolo at Boston College often states, "In science a case is never closed." The author generally agrees with this statement and especially as it applies to this "final problem".